**Journal of Natural Resources and Environmental Management**
https://dx.doi.org/10.29244/jpsl.16.4.494

RESEARCH ARTICLE

OPEN ACCESS

Check for updates

# Detecting Flood Inundation using a Multi-Threshold Overlay Approach and Its Relationship with the Land Cover in Pontianak

Boy Rangga[a], Hervian Handika Sugasta[b], Doddy Cahyadi Saputra[b]

[a] Department of Environmental Engineering, Faculty of Engineering, Tanjungpura University, Pontianak, 78124, Indonesia.
[b] Department of Civil Engineering, Faculty of Engineering, Tanjungpura University, Pontianak, 78124, Indonesia.

**Article History**
Received 3 November 2025
Revised 14 June 2026
Accepted 29 June 2026

**Keywords**
flood inundation, google earth engine, land cover, multipe threshold, spatial planning



**ABSTRACT**

Pontianak is a lowland area prone to flooding driven by hydrological factors, topographical conditions, and land cover changes. This study analyzed flood inundation using a Multi-Threshold Overlay approach based on Sentinel-1 SAR imagery and examined its relationship with land cover classified from Sentinel-2 MSI imagery using the Random Forest algorithm on the Google Earth Engine. This study assumes that the Multi-threshold Overlay approach improves flood detection reliability by identifying areas consistently detected across multiple threshold values. The relationship between flood inundation and land cover was analyzed using spatial overlay and regression analysis. The results showed that the land cover classification achieved an Overall Accuracy of 78.82% (κ = 0.706), while the flood inundation detection attained an Overall Accuracy of 85% (κ = 0.70). The Multi-Threshold Overlay approach identified 1,335.86 ha of flood inundation and generated consistent inundation areas across all threshold values (1.05–1.25). The consistent identification of inundated areas across multiple threshold values suggests that integrating threshold values can improve the reliability of flood inundation mapping. Overlay analysis indicated that infrastructure areas accounted for 49.8% of the total inundated area, followed by agricultural/plantation areas (26.0%) and vegetation cover (24.2%). Regression analysis further confirmed a strong positive relationship between land cover and flood inundation extent ($R^2$ = 0.875; r = 0.93). These findings suggest that the dominance of built-up areas increases the risk of flood inundation, highlighting the importance of infiltration space, sustainable drainage systems, and blue-green infrastructure in spatial planning.

## Introduction

Flooding and urban inundation are among the most frequent hydrometeorological disasters. These disasters are rapidly increasing with the expansion of built-up areas and changes in land cover. In addition to these factors, topographic characteristics play a crucial role in determining whether a region is susceptible to flooding. The city of Pontianak is known for its low elevation [1], which is vulnerable to flooding and inundation, especially during the rainy season [2]. Furthermore, suboptimal urban drainage and high rainfall intensity [3] intensify flooding and inundation as the main problems faced by the community in Pontianak [4]. However, the massive development of buildings and population growth have also changed the land cover [5] and reduced the green open space area, which has led to an increase in the surface runoff volume and directly affected inundation and flooding [6]. These conditions underscore the need to examine the spatial patterns of flood inundation alongside land cover characteristics in Pontianak.

Geographic Information Systems (GIS) have become important tools for monitoring and analyzing flood events across both space and time [7]. Among the available remote sensing datasets, Sentinel imagery provides 10 m spatial resolution and spectral characteristics well suited for flood mapping [8]. Sentinel-1 SAR imagery is particularly valuable because it can acquire data regardless of cloud cover or weather conditions.

**Corresponding Author:** Boy Rangga boyrangga1992@teknik.untan.ac.id Department of Environmental Engineering, Faculty of Engineering, Tanjungpura University, Pontianak, 78124, Indonesia.

Flood inundation is commonly detected using change detection techniques that identify surface changes before and after flood events [9]. Combined with analyses of Sentinel-1 backscatter responses, these techniques have demonstrated strong performance in mapping urban flood inundation.

Previous studies have successfully applied Sentinel-1 imagery for flood mapping, but most have relied on either a single threshold or independent evaluations of multiple threshold values [9,10]. Such approaches assume that one threshold adequately represents inundation conditions or compare thresholds separately without considering their spatial agreement. As a result, mapped inundation areas can vary substantially depending on the selected threshold, while the consistency of inundation patterns across multiple threshold scenarios remains insufficiently explored, particularly in low-lying urban environments. Moreover, although flood inundation mapping has been widely investigated, fewer studies have quantitatively examined how inundation patterns relate to land cover characteristics.

To address these limitations, this study applies a Multi-Threshold Overlay approach that integrates Sentinel-1 threshold values ranging from 1.05 to 1.25 to identify inundated areas consistently detected across multiple threshold scenarios. Rather than relying on a single threshold, the approach evaluates whether areas repeatedly identified as inundated provide a more spatially consistent representation of flood-prone locations. The analysis was implemented on the Google Earth Engine (GEE) platform, which enables efficient processing of large geospatial datasets [11].

In addition to mapping flood inundation, this study quantifies the relationship between inundation distribution and land cover using spatial overlay analysis, the coefficient of determination ($R^2$), and the correlation coefficient (r). Linking inundation patterns with land cover provides a clearer understanding of how different land-use types influence flood occurrence in lowland urban environments. The results also identify land cover categories that are most affected by flooding, offering information that can support urban planning and flood risk management in Pontianak. These findings may assist decision-makers in prioritizing urban growth management, preserving green open space, and promoting ecosystem-based infrastructure to strengthen climate adaptation and reduce future flood risk.

This research addresses these gaps by combining Multi-Threshold Overlay analysis of Sentinel-1 SAR imagery with land cover classification derived from Sentinel-2 MSI imagery and the Random Forest algorithm. Specifically, it (1) maps flood inundation across Pontianak, (2) classifies the city's land cover, and (3) evaluates the relationship between inundation patterns and land cover using spatial overlay, the coefficient of determination ($R^2$), and the correlation coefficient (r). The results provide an empirical basis for improving urban flood mitigation and supporting more sustainable land-use planning in lowland cities [12].

## Materials and Methods

### Research Location

Geographically, Pontianak extends from 0°02'24" N to 0°05'37" S latitude and from 109°16'25" to 109°23'04" E longitude, placing it directly on the equator. Its equatorial location contributes to a humid tropical climate characterized by abundant annual rainfall and consistently high temperatures throughout the year [13]. Pontianak, the capital of West Kalimantan Province, Indonesia, was selected as the study area because of its high susceptibility to flooding. The city occupies approximately 11,832 hectares and is divided administratively into six sub-districts and 29 neighborhoods. In 2023, Pontianak had a population of 682,728, corresponding to a population density of about 6,331 people per km², making it one of the most densely populated urban centers in West Kalimantan [14].

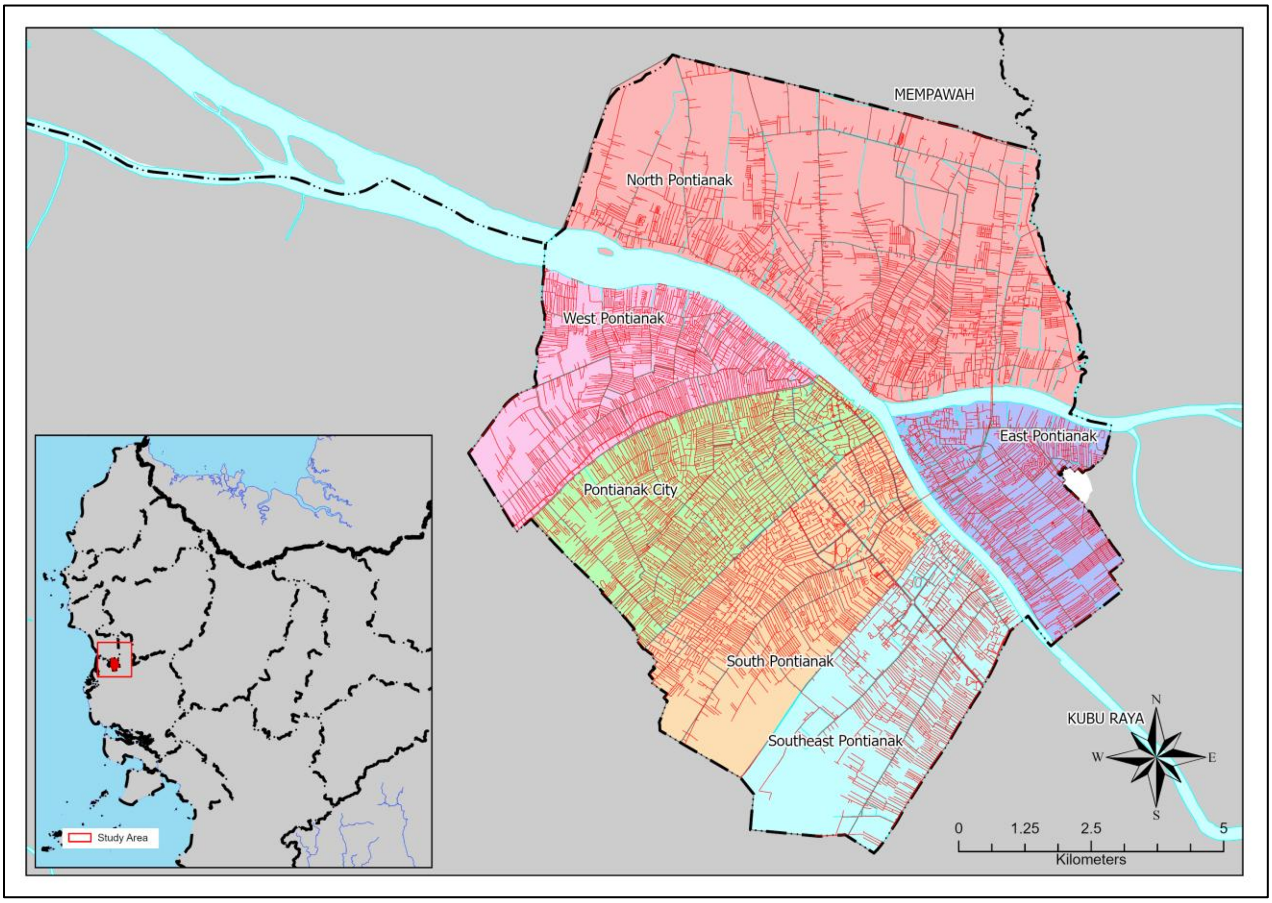


**Figure 1.** Map of Pontianak City, West Kalimantan, Indonesia, showing the study area. The figure presents the location of Pontianak City within West Kalimantan Province and the administrative boundaries of the six districts that constitute the study area. This map provides the geographical context for the research and identifies the spatial extent used for flood inundation and land cover analyses

**Data Collection**

This study utilized satellite imagery from Sentinel-1 SAR GRD (C-band Synthetic Aperture Radar) to analyze flood-affected areas in Pontianak and Sentinel-2 MSI (Multispectral Instrument) to assess land cover conditions. Both datasets were accessed and processed using the Google Earth Engine (GEE) platform. In addition to satellite data, records of flooding events in Pontianak were incorporated, with the selected case occurring on July 6, 2023 [15]. To validate the results of the flood and land cover analyses, ground verification was conducted to assess the accuracy of the spatial interpretations.

**Data Analysis**

***Land Cover Analysis***

Land cover classification was conducted using a supervised approach in which training samples were defined for each land cover class to guide the classification process [16]. Sentinel-2 imagery was analyzed using the B4, B3, and B2 band combination on the GEE platform, with the Random Forest algorithm used as the classifier. Random Forest constructs multiple decision trees from the training data and assigns the final class through majority voting [17]. Its ability to handle high-dimensional datasets and model nonlinear relationships among spectral variables makes it suitable for remote sensing applications [18]. Compared with conventional approaches such as Maximum Likelihood Classification (MLC), Random Forest does not require assumptions about the statistical distribution of the input data and has consistently produced higher classification accuracy for multispectral imagery [19]. In this study, the model was trained using 100 decision trees, a configuration selected to achieve reliable classification performance while maintaining computational efficiency [20].

A supervised classification strategy was adopted in which training samples defined the spectral characteristics of each land cover category. Because Sentinel-2 imagery has a spatial resolution of 10 m, individual pixels may contain multiple surface features, resulting in mixed pixels that reduce the discrimination of spectrally similar land cover types. To minimize this limitation, the classification scheme was grouped into four broad categories: water bodies, infrastructure, agriculture/plantation, and vegetation. Although simplified, these classes are appropriate for the spatial resolution of Sentinel-2 imagery and adequately represent the land cover patterns required for subsequent flood inundation analysis. Classification accuracy was assessed using a confusion matrix. The required number of validation samples was calculated using Equation 3, after which samples were allocated proportionally to the area of each land cover class to ensure adequate representation across all categories. In the confusion matrix, columns correspond to the reference classes, whereas rows represent the classes predicted by the classifier. The overall workflow for land cover analysis is presented in Figure 2.

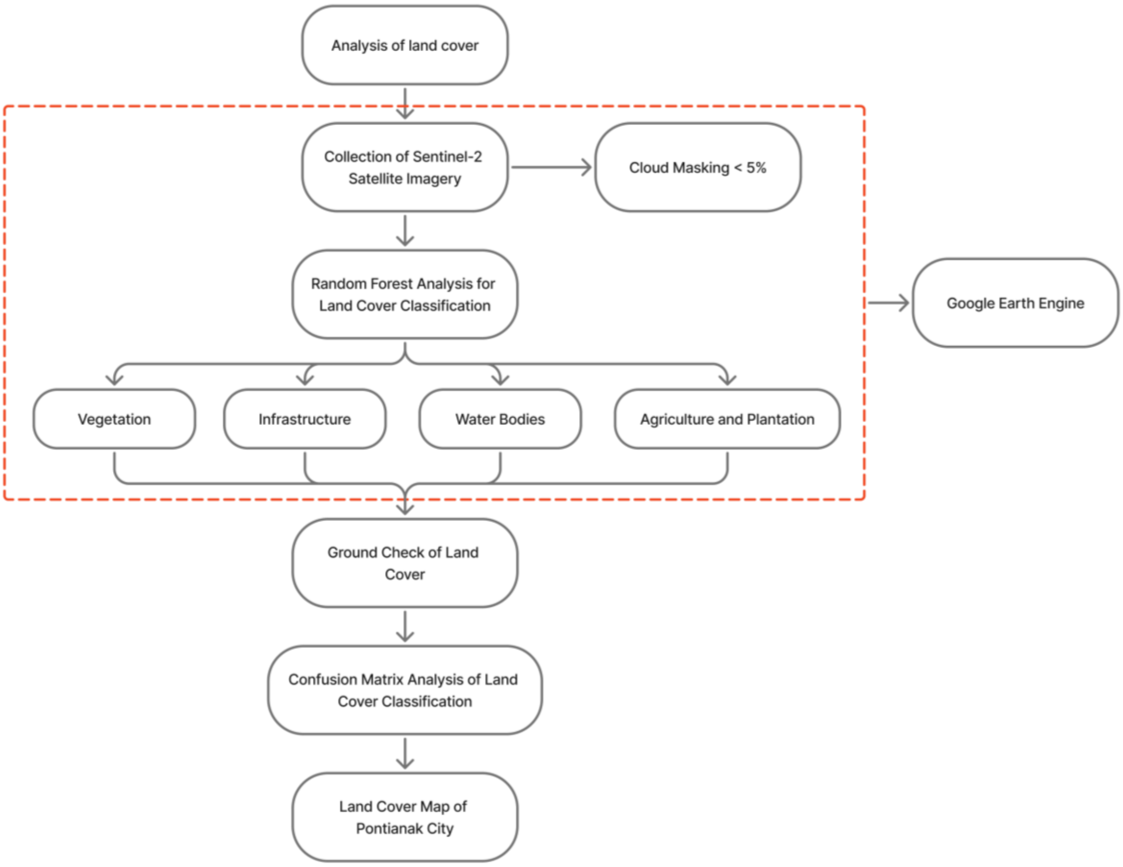


**Figure 2**. Flowchart illustrating the land cover classification process. It outlines the steps such as Sentinel-2 image acquisition, cloud masking, feature extraction, training the Random Forest model, classification, validation, and generating the land cover map. This map was used for overlay and regression analyses with flood inundation data obtained from Sentinel-1 SAR images.

***Flood Inundation Analysis***

Satellite imagery was first clipped to the administrative boundary of Pontianak before flood inundation analysis was performed using Sentinel-1 Ground Range Detected (GRD) C-band Synthetic Aperture Radar (SAR) imagery. Unlike optical sensors such as Landsat, Sentinel-1 can acquire observations regardless of cloud cover or daylight conditions, making it well suited for flood monitoring in tropical regions where persistent cloud cover often limits optical imagery. Nevertheless, radar observations in densely built urban areas may be affected by double-bounce scattering, which produces complex backscatter responses. To take advantage of the strengths of both sensors, Sentinel-1 was used for flood inundation detection, whereas Sentinel-2 imagery was employed for land cover classification.

Image quality was improved by applying a Lee filter to suppress speckle noise, a characteristic granular pattern in SAR imagery. Flood inundation was then identified by comparing pre-flood and post-flood Sentinel-1 images. Because the Sentinel-1 GRD dataset available through GEE is distributed with standard preprocessing, including radiometric calibration and terrain correction, no additional corrections were required before analysis. Sentinel-1 GRD imagery has a spatial resolution of 10 meters, while Sentinel-2 includes bands with 10-meter (B2, B3, B4, B8) and 20-meter (B5, B6, B7, B8A, B11, B12) resolutions. Land cover classification was based on the B4, B3, and B2 band combination. The Lee filter was implemented using Equation 1 to reduce speckle noise and improve the interpretability of the radar imagery [21]:

$$Y_{ij} = \overline{K} + W\ x\ (C - \overline{K}) \quad (1)$$

Description:
$Y_{ij}$ : despeckled image
$\overline{K}$ : Kernel/scene average
W : weighting
C : center element in kernel/scene

Pre-flood and post-flood Sentinel-1 SAR images were selected to capture surface conditions before and after the flood event. Changes in radar backscatter between the two acquisition dates formed the basis for flood inundation detection. Operating in the C-band, Sentinel-1 is particularly sensitive to variations in surface moisture and open water, allowing flooded areas to be distinguished from surrounding land surfaces through changes in backscatter intensity. Flood inundation was identified using a change detection approach with threshold values of 1.05, 1.10, 1.15, 1.20, and 1.25 following the methodology of [9]. Previous research reported overall classification accuracies ranging from 81.13% to 94.34% for this threshold range when applied to Sentinel-1 SAR imagery [9]. Based on a prior study, this range produced overall accuracy values between 81.13% and 94.34% using Sentinel-1 SAR imagery [9]. Accordingly, these thresholds were adopted to represent different flood detection scenarios and were further evaluated within the study area to examine the sensitivity of inundation mapping to threshold selection. A Multi-Threshold Overlay approach was then applied to integrate the individual detection results. Each threshold-derived inundation map was converted to a binary layer in which inundated pixels were assigned a value of 1. Because each threshold represented an equivalent detection scenario, all layers received equal weight. The binary layers were subsequently overlaid and summed, producing scores from 0 to 5 that reflected the frequency with which individual pixels were identified as inundated. Pixels receiving the maximum score of 5 were classified as flood inundation areas because they were consistently detected across all threshold scenarios.

To reduce false positives, areas with slopes greater than 5% were excluded using the 30 m SRTM Digital Elevation Model (DEM), as this threshold has been reported to improve classification accuracy [22]. Permanent water bodies, particularly the Kapuas River, were also masked from the inundation maps using ArcGIS before the overlay analysis was finalized. Overall classification accuracy was subsequently evaluated using Equation 2 [23]:

$$OA = \frac{\sum_{i=1}^{k} nii}{N} x100\% \quad (2)$$

Description:
nii : number of correct samples
N : total number of samples

A limited sensitivity analysis was performed by comparing flood inundation extents derived from threshold values between 1.05 and 1.25. Other factors that may influence inundation mapping, including image acquisition dates, rainfall conditions, tidal dynamics, and drainage capacity, were not evaluated in the present study. Because these variables can affect both flood extent and its spatial distribution, incorporating them into future analyses would provide a more rigorous assessment of the method's reliability under different hydrological and urban conditions.

***Ground Check on Land Cover and Flood Inundation***

Field verification was conducted to assess the agreement between satellite-derived land cover classifications and flood inundation maps and the corresponding ground conditions [24]. The observations collected during the ground survey were used to evaluate classification performance and to provide reference data for the confusion matrix and subsequent accuracy assessment. Ground check locations were determined using a stratified random sampling approach, with the required number of samples calculated according to Equation 3 [25].

$$N = (\sum i = 1(W_i\, xS_i)/S_o)^2 \tag{3}$$

Description:
Wi : proportion of class i areas mapped
Si : standard deviation of strata i
So : standard deviation expected from overall accuracy

The number of ground-check points was determined using the sampling equation and therefore depended on the spatial extent of each analysis area. As a result, smaller analysis areas required fewer validation points for both flood inundation and land cover assessments, which may have limited the representation of the full range of inundation conditions across Pontianak. This limitation may affect the uncertainty in the accuracy assessment results, particularly in areas that are difficult to access or where inundation conditions are temporary and highly dynamic. Accuracy was assessed using overall accuracy, user accuracy, producer's accuracy, and the kappa coefficient (confusion matrix). The confusion matrix is a common method for testing remote sensing accuracy by comparing the relationship between known field data and processed results. The flowchart of the inundation detection analysis is shown in Figure 3.

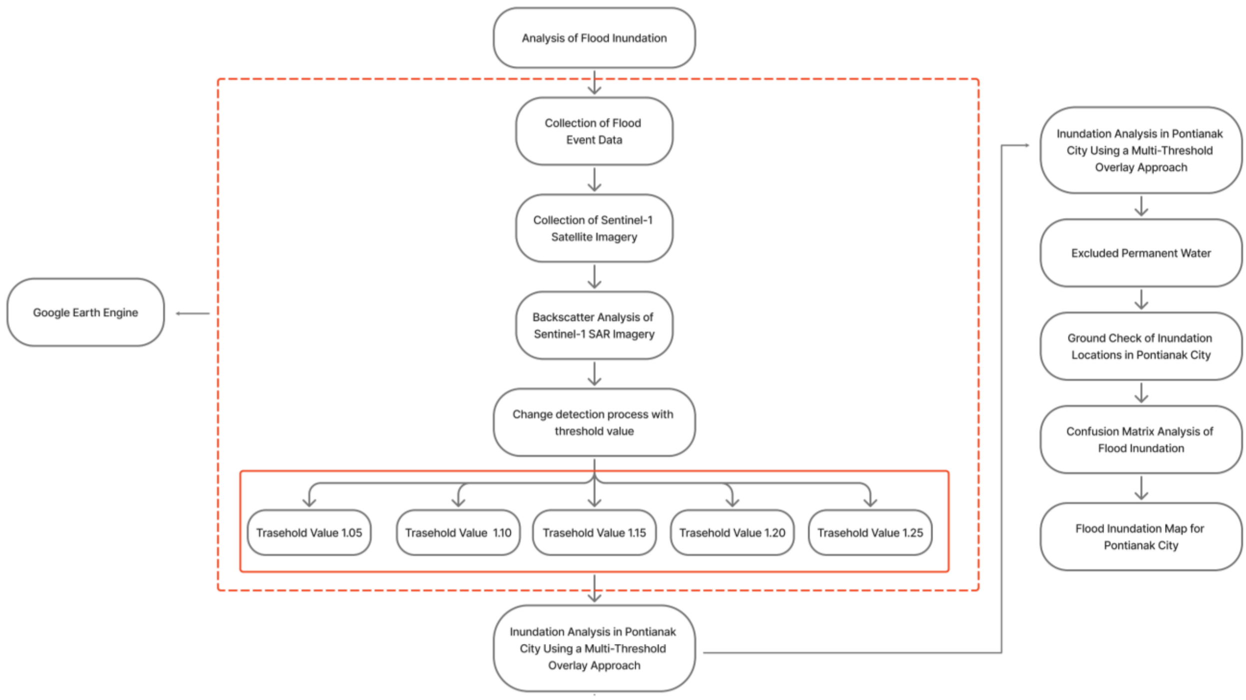


**Figure 3**. Flowchart illustrating the flood inundation detection process with the Multi-Threshold Overlay method. It outlines the steps from Sentinel-1 SAR image acquisition and preprocessing to applying various threshold values, overlaying inundation results, and validating the final flood map. The resulting map highlights areas consistently identified across thresholds and was used to analyze the link between flood inundation and land cover.

***Overlaying Land Cover and Flood Inundation Maps***

Overlay is a GIS-based analytical method that integrates multiple spatial data layers to examine geographic phenomena that occur simultaneously. It facilitates descriptive, deductive, and inductive analyses and is commonly utilized in change analysis, spatial accuracy assessment, and multi-criteria evaluation through both geometric and arithmetic methods [26]. In this study, overlay analysis was applied for change analysis, which identifies and measures temporal changes by comparing different data layers. The overlay combined processed land cover and flood inundation data to determine the flood-affected land cover types. The results were quantitatively analyzed using the coefficient of determination ($R^2$) to examine the relationship between each land cover classification and flood inundation area. $R^2$ was calculated using Equation 4.

$$R^2 = 1 - \frac{\sum_{i=1}^{n}(y_i - \widehat{y_i})^2}{\sum_{i=1}^{n}(y_i - \bar{y})^2} \tag{4}$$

$R^2$ is the coefficient of determination, which indicates the proportion of the observed variation explained by the regression model. $y_i$ represents the observed value for the "i" observation, where $\widehat{y_i}$ denotes the corresponding predicted value generated by the regression model. $\bar{y}$ represents the mean of all observed values and is used as a reference when calculating the total variation in the data. $n$ denotes the total number of observations used in the analysis. These variables are used to calculate the coefficient of determination $R^2$, which provides a measure of the regression model's ability to explain the relationship between the variables under analysis. To determine the strength of the relationship between variables, the Pearson correlation coefficient (r) was calculated using Equation 5.

$$r = \sqrt{R^2} \tag{5}$$

Where:
$r$ = Pearson correlation coefficient

## Results and Discussion

### Results

#### *Flood Inundation Analysis Result*

Flood inundation is driven by multiple interacting factors, including rainfall intensity, land cover, topography, and drainage capacity. Information on the spatial distribution of inundation is essential for understanding an area's susceptibility to flooding. In this study, flood inundation was identified using a change detection approach that compared surface conditions before and after a flood event. Based on this approach, the results of the change detection analysis for the study area are shown in Figure 4.

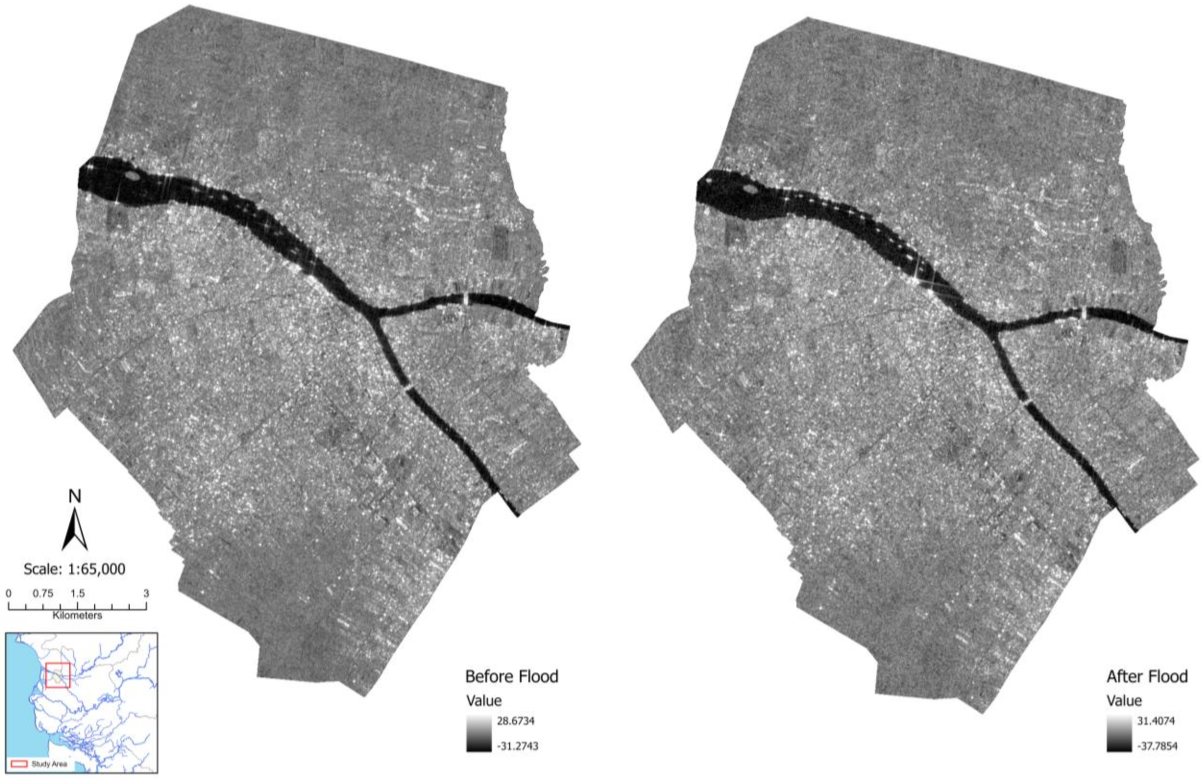


**Figure 4.** Satellite images show the area before (left) and after (right) the flood in Pontianak City, West Kalimantan, Indonesia. They depict surface conditions prior to and following the flood, offering visual context for the inundation patterns observed. These datasets served as the foundation for flood analysis and comparison with land cover distribution.

Satellite imagery was used to analyze flood inundation in Pontianak. Water inundation was detected by comparing pre- and post-event images [27]. An increase in backscatter values was observed in both pre-flood and post-flood imagery [28], likely due to surface conditions such as vegetation and soil, which typically produce higher radar reflectance [29]. Change detection was performed using a set of predefined threshold values. This was followed by an extraction process to identify the spatial distribution of flood inundations. Five threshold values were applied in this study: 1.05, 1.10, 1.15, 1.20, and 1.25. Permanent water bodies were removed from the analysis by masking the Kapuas River prior to change detection, improving the accuracy of flood classification by eliminating responses from pre-existing water surfaces. Flood inundation extents estimated for each threshold value are presented in Table 1 and depicted in Figure 5.

**Table 1.** Flood inundation zones corresponding to each threshold in the Multi-Threshold Overlay analysis are presented. The table details flood extents derived from Sentinel-1 SAR imagery, with ratio thresholds between 1.05 and 1.25 in Pontianak City. This comparison illustrates how different threshold values influence the flood extent mapping and helps identify reliably detected areas for subsequent analysis.

| No. | Threshold | Area (hectares) |
|---|---|---|
| 1 | 1.05 | 3,313.46 |
| 2 | 1.10 | 2,703.73 |
| 3 | 1.15 | 2,163.28 |
| 4 | 1.20 | 1,711.12 |
| 5 | 1.25 | 1,335.86 |

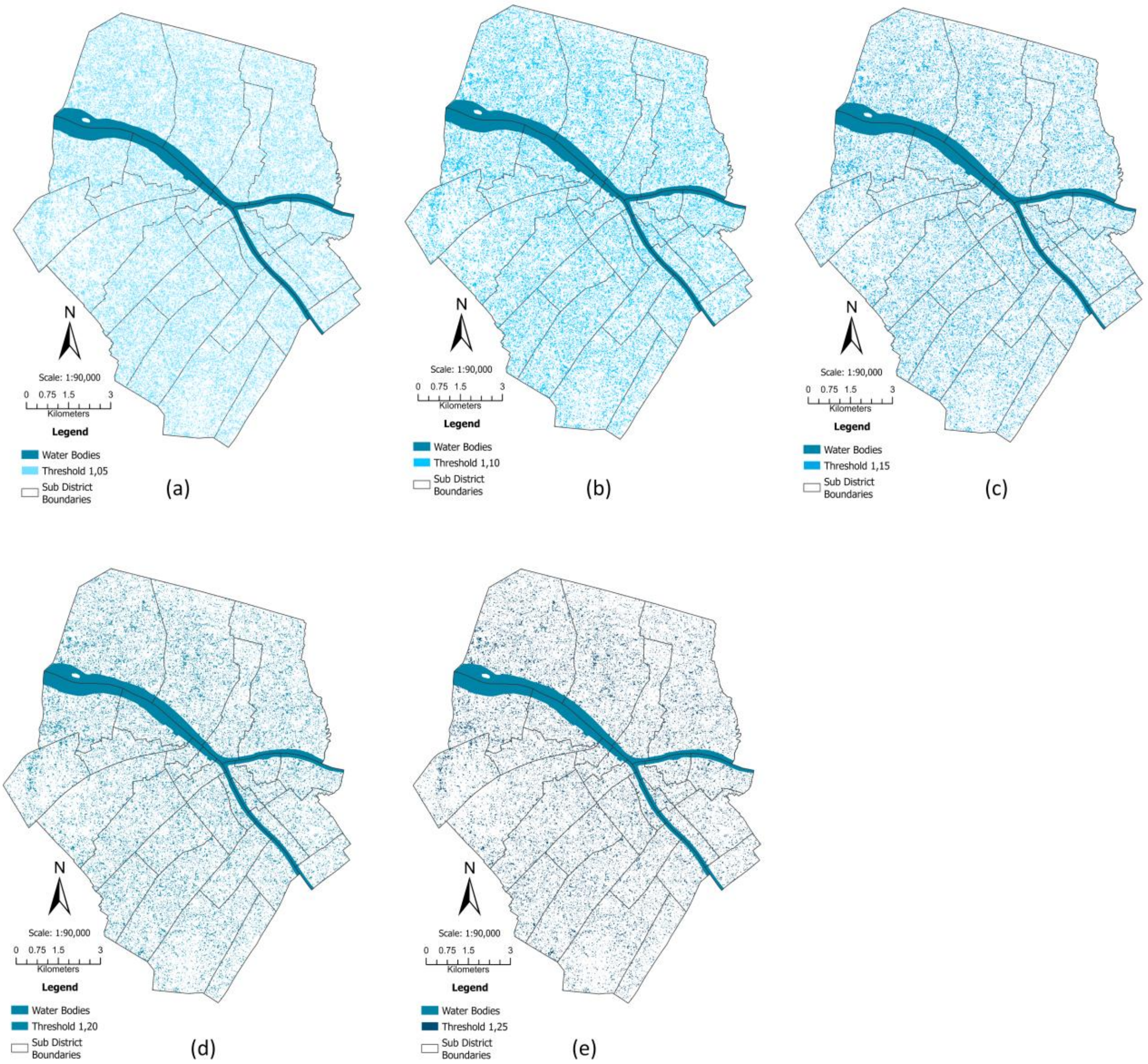


**Figure 5.** Flood inundation maps are generated with five threshold values: 1.05 (a), 1.10 (b), 1.15 (c), 1.20 (d), and 1.25 (e). Each map shows the flood extent identified from Sentinel-1 SAR imagery in Pontianak City using different thresholds in the Multi-Threshold Overlay method. Comparing these maps reveals how sensitive flood detection is to the chosen threshold and helps identify areas that are consistently inundated, which are used in the final flood map.

Following this step, the individual inundation maps were integrated using the Multi-Threshold Overlay approach. The analysis estimated a total flood inundation extent of 1,335.86 ha across Pontianak. Notably, this extent was identical to the inundation area obtained using the 1.25 threshold, indicating that all pixels detected at this threshold were consistently identified across the entire threshold range (1.05–1.20). Consequently, only pixels classified as inundated under every threshold scenario were retained in the final map (cumulative score = 5). This result demonstrates that the 1.25 threshold produced the most spatially consistent inundation pattern among the thresholds evaluated. The overlay approach employed in this study serves as a spatial verification mechanism to identify inundated areas consistently detected across multiple threshold scenarios. Thus, the method reduces the likelihood of misclassification associated with the use of a single threshold and enhances the reliability of the flood inundation mapping results. To assess the reliability of the results, the overall accuracy was calculated using ground verification points within the inundated zones. The results of the multi-threshold overlay analysis are presented below, and the maps and ground check map of the flood-affected area are presented in Figure 6.

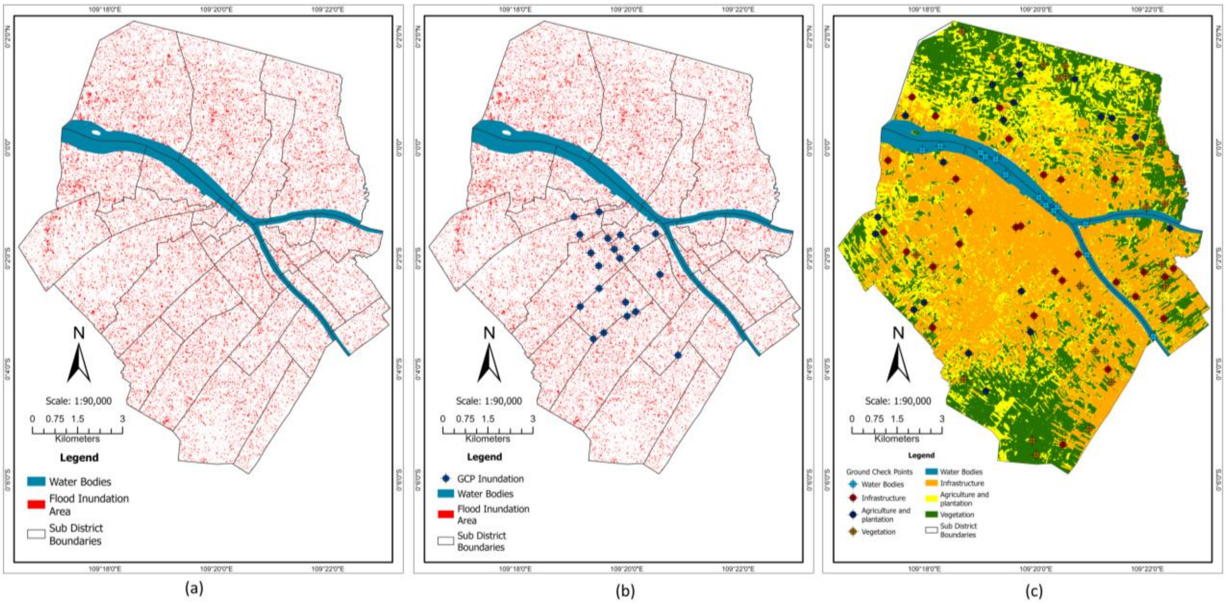


**Figure 6.** Map of multi-threshold overlay flood analysis (a), Map of ground check on (b) multi-threshold overlay flood analysis, and Land Cover (c). The flood inundation map was generated from Sentinel-1 SAR imagery using the Multi-Threshold Overlay approach, while the land cover map was produced from Sentinel-2 MSI imagery using the Random Forest algorithm. Together, these maps illustrate the validated flood inundation results and the spatial distribution of land cover used to analyze the relationship between flood occurrence and land cover in Pontianak, West Kalimantan, Indonesia.

Ground verification was conducted by observing actual inundated locations and comparing them with flood analysis results. In this study, 20 ground checkpoints were selected across the inundated and non-inundated areas. Field observation data were subsequently used as reference data for accuracy assessment. Furthermore, the accuracy of the flood-inundation mapping results for Pontianak was evaluated using a confusion matrix to obtain the overall accuracy, producer's accuracy, user's accuracy, and Kappa coefficient. The overall accuracy of the flood inundation in Pontianak was calculated using a confusion matrix. The results are shown in Table 2.

**Table 2.** Confusion Matrix of Flooded Areas in Pontianak. This table compares flood inundation classifications obtained from the Multi-Threshold Overlay method with Sentinel-1 SAR imagery and ground validation data. The results serve as a basis for calculating overall accuracy, producer's accuracy, user's accuracy, and Cohen's kappa coefficient, illustrating the reliability of the flood detection.

| Confusion Matrix | | Data | | Row Totals | UA (%) | CE (%) |
|---|---|---|---|---|---|---|
| | | Inundation | Non-inundation | | | |
| Accuracy Result | Inundation | 9 | 1 | 10 | 90 | 10 |
| | Non-inundation | 2 | 8 | 10 | 20 | 80 |

| Confusion Matrix | Data | | Row Totals | UA (%) | CE (%) |
|---|---|---|---|---|---|
| | Inundation | Non-inundation | | | |
| Column Totals | 11 | 9 | 20 | 55 | 45 |
| PA (%) | 82 | 89 | OA (%) | 85.00 | |
| OE (%) | 18 | 11 | k | 0.70 | |

The accuracy of flood inundation classification was assessed using a confusion matrix, yielding a user accuracy (UA) of 90% for the inundation class, indicating that 90% of the area identified as flooded was confirmed to be inundated in the field. Moreover, the Producer's accuracy (PA) was 82%, signifying that 82% of the actual flooded area was accurately identified by the model, and the Overall Accuracy (OA) was 85%, indicating a strong agreement with the reference data. The Kappa coefficient (κ = 0.70) indicates substantial agreement, supporting the reliability of the flood inundation classification [30].

Flood inundation in Pontianak was concentrated primarily in built-up urban areas characterized by low elevations and relatively flat terrain. The Multi-Threshold Overlay approach identified 1,335.86 ha of inundated land, with the same inundation extent retained across all evaluated threshold values (1.05–1.25). The persistence of these inundated pixels across every threshold scenario indicates that they represent consistently detected flood-prone areas rather than threshold-dependent classifications, demonstrating that the Multi-Threshold Overlay approach reduces the sensitivity of inundation mapping to the choice of a single threshold.

***Land Cover Analysis Result***

Land cover in Pontianak was classified from Sentinel-2 imagery using a supervised classification approach based on training samples representing predefined land cover categories. The procedure distinguished water bodies, vegetation, rice fields, built-up areas, and open land according to their spectral characteristics. The resulting land cover map was subsequently used to quantify the spatial distribution and proportion of each class and to examine its relationship with flood inundation. The Sentinel-2 Multispectral Instrument (MSI) imagery used for the analysis is shown in Figure 7.

Land cover classification was carried out in GEE using the workflow described in the methodology. Training samples represented four land cover categories: water bodies, infrastructure (built-up areas), agriculture/plantation, and vegetation. The resulting land cover map is presented in Figure 7. The classified map indicates that Pontianak covers approximately 11,832.00 ha and is dominated by infrastructure, which occupies 5,155.22 ha (43.57%) of the total area. Vegetation accounts for 3,206.47 ha (27.10%), followed by agricultural and plantation land covering 2,797.31 ha (23.64%). Water bodies represent the smallest class, occupying 673.00 ha (5.69%).

The spatial distribution of these land cover classes reflects the city's pattern of urban development. Infrastructure is concentrated primarily within the urban core and along major transportation corridors that connect commercial, residential, and service areas. Vegetation is more extensive in the peripheral parts of the city, where urban development is less intensive. In this study, the vegetation class includes natural vegetation, shrubland, urban green spaces, and small remnants of forest located within the peri-urban zone. Agricultural and plantation land is also concentrated toward the city's outskirts, particularly near the boundary with Kubu Raya Regency, and consists mainly of cultivated fields and community-managed plantations. Together, these patterns illustrate a transition from densely developed urban areas to landscapes with greater vegetation cover and agricultural land toward the city's periphery.

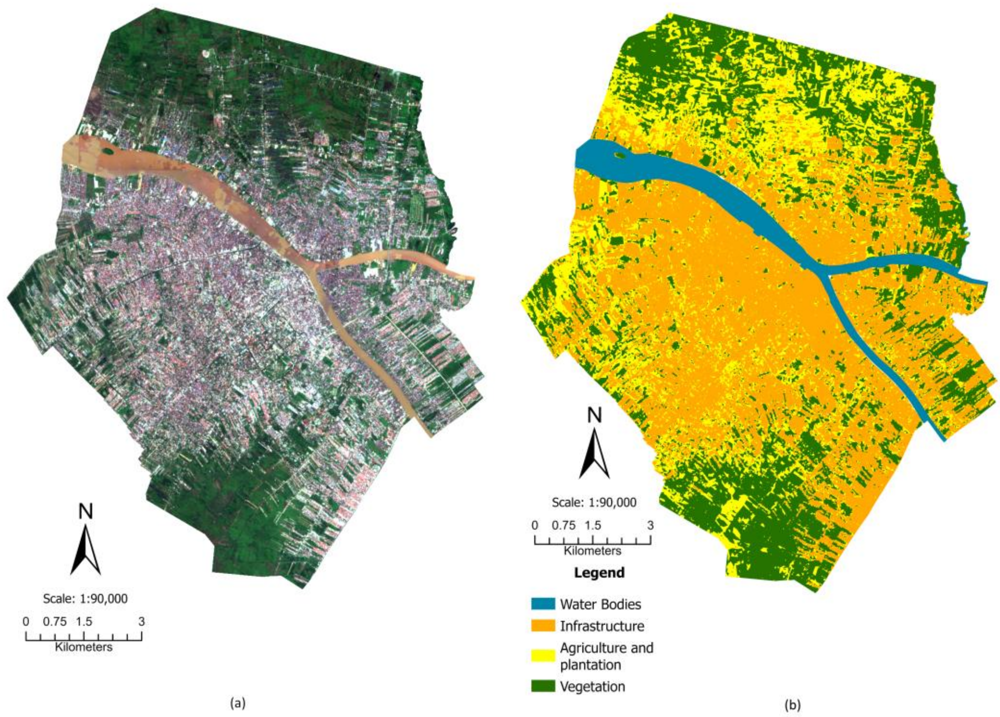


**Figure 7.** Sentinel-2 multispectral image of Pontianak in 2024 (a) and the land cover classification map for Pontianak (b). The figure shows the satellite source data and the land cover map created with the Random Forest algorithm in GEE. The classified map illustrates the distribution of key land cover types and functions as the main dataset for examining the link between land cover and flood inundation.

Land cover classification was validated through field verification using ground-check locations selected by stratified sampling. Observations from these sites were used to construct the confusion matrix and evaluate classification accuracy. The allocation of validation points for each land cover class is summarized in Table 3.

Table 3. Confusion Matrix Results for Land Cover Classification. The table compares land cover classes classified from Sentinel-2 Multispectral Instrument (MSI) imagery using the Random Forest algorithm with the reference data collected for validation. The resulting accuracy metrics, including overall accuracy, producer's accuracy, user's accuracy, and Cohen's kappa coefficient, demonstrate the reliability of the land cover classification used in the subsequent flood inundation analysis.

| Confusion Matrix | | Number Of Ground Check Points | Data | | | | Row Totals | UA (%) | CE (%) |
|---|---|---|---|---|---|---|---|---|---|
| | | | Water bodies | Infrastructure | Agriculture | Vegetation | | | |
| Accuracy Result | Water bodies | 13 | 13 | 0 | 0 | 0 | 13 | 100 | 0 |
| | Infrastructure | 29 | 0 | 29 | 7 | 3 | 39 | 74 | 26 |
| | Agriculture | 21 | 0 | 1 | 11 | 3 | 15 | 73 | 27 |
| | Vegetation | 21 | 0 | 0 | 4 | 14 | 18 | 78 | 22 |
| Column Totals | | 85 | 13 | 30 | 22 | 20 | 85 | | |
| PA (%) | | | 100 | 97 | 50 | 70 | OA (%) | 78.824 | |
| OE (%) | | | 0 | 3 | 50 | 30 | k | 0.706 | |

The confusion matrix indicated good classification performance, with an Overall Accuracy (OA) of 78.82% and a Kappa coefficient (κ) of 0.706, representing substantial agreement [30]. Among the four land cover classes, water bodies achieved perfect classification accuracy, with both Producer's Accuracy (PA) and User's Accuracy (UA) of 100%. Infrastructure also performed well, recording a PA of 97% and a UA of 74%; the lower UA suggests that some non-infrastructure areas were classified as built-up surfaces because of similar spectral responses. Agriculture produced the lowest PA (50%) and a UA of 73%, whereas vegetation achieved a PA of 70% and a UA of 78%. Misclassification between agricultural land and vegetation was likely caused by their similar spectral characteristics in Sentinel-2 imagery and the 10 m spatial resolution, which limits the discrimination of fine-scale land cover features. Despite these class-specific differences, the overall accuracy statistics indicate that the classified land cover map provides a reliable basis for examining the spatial relationship between flood inundation and land cover in Pontianak.

The classified land cover map also highlights a distinct spatial pattern across Pontianak. Infrastructure is concentrated within the urban core and along major transportation corridors that support commercial, residential, and service activities. In contrast, vegetation and agricultural/plantation land are distributed mainly in the city's peripheral areas, particularly near the boundary with Kubu Raya Regency. This transition from densely built urban areas to greener suburban landscapes reflects the city's pattern of urban expansion and is likely to influence local hydrological processes by increasing surface runoff in highly developed areas.

***Land Cover Overlay and Flood Inundation Area***

Spatial overlay analysis was performed to examine how flood inundation was distributed across the major land cover classes in Pontianak. The resulting overlay map and the corresponding distribution of inundated areas are presented in Figure 8. Infrastructure accounted for the largest inundated area, covering 675.30 ha, or approximately 49.8% of the total flood extent. Agricultural and plantation land ranked second with 351.86 ha, followed closely by vegetation with 328.70 ha. The relatively small difference between the latter two classes indicates that flood inundation extended beyond built-up areas into surrounding non-urban landscapes.

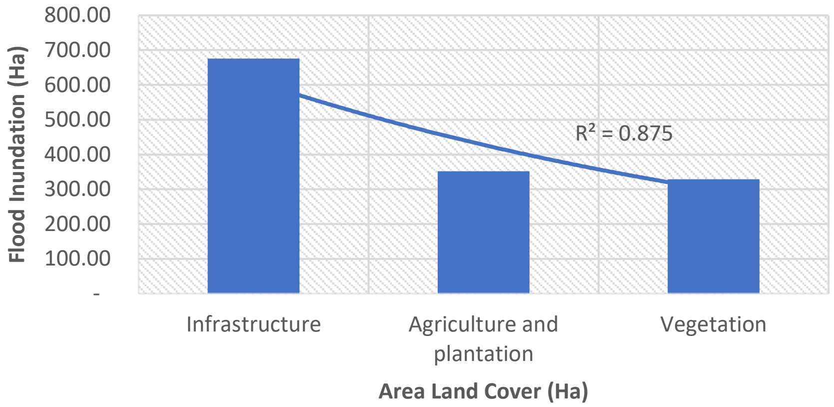


**Figure 8.** Histogram depicting Inundation Area versus Land Cover in Pontianak City, along with the R2 coefficient indicating the correlation between flood inundation and land cover. The figure summarizes the spatial overlay and regression analysis results conducted in Pontianak City using flood and land cover data.

The relationship between land cover area and flood inundation was further evaluated using the coefficient of determination and the correlation coefficient (Equations 4 and 5). Regression analysis produced an $R^2$ value of 0.875, indicating that 87.5% of the variation in flood inundation area could be explained by differences in land cover area at the aggregated class level. The corresponding correlation coefficient ($r = 0.93$) demonstrates a strong positive relationship between the two variables. Together with the overlay analysis, these results indicate that infrastructure areas experienced the greatest flood inundation, consistent with the influence of extensive impervious surfaces on surface runoff and flood susceptibility in Pontianak.

## Discussion

The predominance of infrastructure in Pontianak reflects the city's continuing urban expansion and provides an important context for interpreting the observed flood inundation patterns. This result is consistent with the findings of [5], who documented a progressive increase in built-up areas associated with urban development. Conversely, the presence of vegetation and relatively extensive agricultural land indicates that some areas still function as water catchment zones. The observed inundation characteristics are also related to the relatively flat topography of Pontianak City and the dominance of built-up areas, both of which can increase the surface runoff.

The flood inundation analysis employed a Multi-Threshold Overlay approach to address the uncertainty commonly associated with the use of a single threshold in Sentinel-1 SAR-based change detection. In backscatter ratio-based flood mapping, threshold selection is a critical factor that influences the classification results. Threshold values that are too low tend to produce larger inundated areas because they are more sensitive to minor changes in backscatter values. Meanwhile, excessively high threshold values may exclude portions of the actual inundated areas owing to stricter classification criteria. Therefore, the use of multiple threshold values is expected to yield a more representative and reliable delineation of flood inundation than conventional single-threshold methods. A key advantage of the Multi-Threshold Overlay approach over conventional single-threshold methods is its ability to evaluate the consistency of flood inundation detection across different sensitivity levels. In a single-threshold approach, the classification results depend heavily on the selected threshold, which may lead to either overestimation or underestimation of the inundation extent. In contrast, the Multi-Threshold Overlay approach integrates inundation maps generated from multiple threshold values, allowing inundated areas to be evaluated based on their consistency. Consequently, the method not only produces a flood inundation map but also serves as an internal validation mechanism that reduces the classification uncertainty arising from the selection of a single threshold value.

To examine how flood inundation varied among different land cover types, the classified land cover map was spatially overlaid with the flood inundation map. Infrastructure accounted for the largest share of the inundated area (675.30 ha; 49.8%), followed by agricultural and plantation land (351.86 ha; 26.0%) and vegetation (328.70 ha; 24.2%). These patterns indicate that flood inundation in Pontianak is closely associated with land cover, with built-up areas experiencing the greatest exposure.

The predominance of inundation within infrastructure areas agrees with the findings of [9] who reported frequent flooding in built-up environments characterized by limited infiltration capacity. Similar relationships between urban expansion, increased surface runoff, and reduced drainage efficiency have also been documented elsewhere [31]. Unlike cities where flooding is concentrated in localized depressions, inundation in Pontianak was distributed more broadly across the urban area. This spatial pattern is likely influenced by the city's predominantly low-lying and gently sloping terrain, which limits the concentration of runoff and allows surface water to accumulate over a wider area once drainage capacity is exceeded [32]. Land cover further modifies this topographic influence. Extensive impervious surfaces associated with roads, buildings, and other urban infrastructure reduce infiltration and accelerate runoff generation, increasing the likelihood of flooding throughout the urban core [33], [34], [35]. Although agricultural and plantation land generally has greater infiltration capacity than built-up areas, these landscapes can also become inundated when soils approach saturation. Vegetated areas similarly contribute to flood storage and runoff regulation but remain susceptible to inundation in low-elevation locations and areas adjacent to river channels [36]. Together, these findings suggest that the spatial distribution of flood inundation in Pontianak reflects the combined effects of land cover and topography rather than either factor acting independently.

The result strong positive relationship between land cover area and flood inundation area should be interpreted with caution because the number of analytical units was relatively limited and may not fully represent the spatial variability within the study area. Flood inundation in Pontianak City is strongly associated with land cover patterns. Built-up areas, which dominate nearly half of the inundated region, reflect that urbanization without adequate drainage systems will increase the flood risk [37]. Simultaneously, flooding in agricultural and vegetated areas suggests that additional factors, including hydrological conditions, terrain, and drainage capacity, are influential [38]. Therefore, balanced spatial planning that integrates infrastructure development with the provision of green open spaces and sustainable drainage systems is key to reducing flood risks in Pontianak. Although the regression analysis revealed a strong association between land cover and flood inundation area, this relationship should not be interpreted as evidence that land cover alone determines flood occurrence. In Pontianak, flood inundation is likely shaped by the combined influence of land cover, flat topography, low elevation, drainage capacity, and river system dynamics. The results therefore suggest that expanding built-up areas increase flood susceptibility primarily when they interact with these broader environmental and hydrological conditions.

Nearly half of the mapped inundation (49.8%) occurred within built-up areas, underscoring the influence of impervious surfaces and reduced infiltration capacity on urban flood risk. This pattern highlights the need for adaptive flood management strategies that combine structural and nature-based approaches. Sustainable Urban Drainage Systems (SUDS) [39], including infiltration wells, biopores, infiltration parks, and retention ponds, could help reduce surface runoff, while polder systems [40] are particularly relevant for low-lying cities such as Pontianak. Complementary planning measures should prioritize development control in flood-prone areas, expand permeable surfaces and green open spaces, and promote blue-green infrastructure to strengthen urban resilience. The effectiveness of these interventions also depends on community participation in maintaining drainage networks. The flood inundation and land cover maps generated in this study provide practical evidence for identifying priority areas for flood mitigation and supporting land-use planning and infrastructure investment in the most vulnerable parts of the city.

## Conclusions

This study evaluated a Multi-Threshold Overlay approach using Sentinel-1 SAR imagery to map flood inundation in Pontianak. The analysis identified a total inundated area of 1,335.86 ha and achieved an Overall Accuracy of 85% with a Kappa coefficient (κ) of 0.70, indicating good agreement with the reference data. Consistent inundation patterns were observed across the evaluated threshold range (1.05–1.25), demonstrating that the Multi-Threshold Overlay approach reduces dependence on a single threshold when delineating flood extent. Notably, the final inundation map matched the result obtained with the 1.25 threshold, indicating that this threshold produced the most spatially consistent inundation pattern among those examined.

Land cover classification derived from Sentinel-2 MSI imagery using the Random Forest algorithm achieved an Overall Accuracy of 78.82% and a Kappa coefficient of 0.706. Infrastructure was the dominant land cover class, accounting for 43.57% of the study area, followed by vegetation (27.10%), agriculture/plantation land (23.64%), and water bodies (5.69%). Overlay analysis showed that 49.8% of the mapped inundation occurred within infrastructure areas, while regression analysis identified a strong positive relationship between land cover area and flood inundation area ($R^2 = 0.875$; $r = 0.93$). These results indicate that the spatial distribution of flood inundation in Pontianak is closely associated with land cover, particularly the prevalence of built-up surfaces that limit infiltration and promote surface runoff. Therefore, spatial planning and land use management strategies that incorporate green open spaces, sustainable drainage systems, and blue–green infrastructure should be prioritized to support more adaptive and sustainable flood mitigation efforts in Pontianak.

## Author Contributions

**BR:** Conceptualization, Methodology, Software, Investigation, Writing - Review & Editing; **HHS:** Writing - Review & Editing, and **DCS:** Writing - Review & Editing.

## AI Writing Statement

During the preparation of this work the authors used SCISPACE in order to assist literature review process. After using this tool/service, the authors reviewed and edited the content as needed and took full responsibility for the content of the publication.

## Conflicts of interest

There are no conflicts to declare.

## Acknowledgments

This research was funded by Research and Community Service Institute of Universitas Tanjungpura through the Budget Implementation List Number: SP DIPA-139. 03.2.693380/2025 dated 2 December 2024 in accordance with the Decision of the Rector of Universitas Tanjungpura Number: 1105/UN22/KU.00.01/2025 dated 12 August 2025.

## References


1. Nurhidayati, E. Konsep Blue-Green Infrastructure (BGI) melalui Permeable Pavements Pedestrian dan Kolam Retensi untuk Mitigasi Genangan Banjir di Kota Pontianak. *J. Planol.* **2022**, *19*, 92–110, doi:10.30659/jpsa.v19i1.18043.
2. Xie, L.; Zhao, H. Correlation Between Flood Disaster and Topography: A Case Study of Zhaoqing City. *J. Nat. Disaster* **2013**, *22*, 240–245.
3. Arianti, I.; Rafani, M.; Wattini; Fitriani, N.; Nizar; Vatria, B. Development of an Adaptive Drainage System for Flood Mitigation Using GIS. *Eur. J. Appl. Sci. Eng. Technol.* **2024**, *2*, 81–89, doi:10.59324/ejaset.2024.2(6).07.
4. Farhan, F.I.; Adi, A.C. Forecasting Flood Vulnerability in Pontianak using Multiple Linear Regression and Geospatial Information Systems (GIS). *Innov. Res. Informatics* **2023**, *5*, 9–13, doi: 10.37058/innovatics.v5i1.6567.
5. Nurhidayati, E.; Buchori, I.; Mussadun, M. Prediksi Perkembangan Lahan Permukiman terhadap Kerentanan Bencana Banjir dan Kebakaran di Permukiman Tepian Sungai Kapuas Kota Pontianak. *Tataloka* **2016**, *18*, 249, doi: 10.14710/tataloka.18.4.249-260.
6. Akukwe, T.I. Determinants of Flooding in Port Harcourt Metropolis, Nigeria. *IOSR J. Humanit. Soc. Sci.* **2014**, *19*, 64–72, doi: 10.9790/0837-191186472.
7. Akallouch, A.; Mashoudi, A.A.; Ziani, M.; Elhani, R. GIS Application in Urban Flood Risk Analysis: Midar as a Case Study. *Open J. Ecol.* **2024**, *14*, 148–164, doi: 10.4236/oje.2024.142009.
8. Saputra, A.N.; Nikmah; Wardini, R.; Fitria; Nathania, W.; Misna; Azizah, K.; Ariyadi Analysis of Flood Inundation Mapping Using the Weighting Method in Urban Floods. *IOP Conference Series: Earth and Environmental Science* **2023**, *1276,* 012026.
9. Kenranto, R.A.; Hidayat, H.; Bioresita, F. Analisis Genangan Banjir terhadap Penutup Lahan di Wilayah Tangerang menggunakan Data Citra Sentinel-1 dan Sentinel-2. *JGISE J. Geospatial Inf. Sci. Eng.* **2024**, *7*, 14–22, doi: 10.22146/jgise.87579
10. Bioresita, F.; Hayati, N.; Ngurawan, M.G.R.; Berliana, M. Integrating Insar Coherence and Backscattering for Identification of Temporary Surface Water, Case Study: South Kalimantan Flooding, Indonesia. *Int. Arch. Photogramm. Remote Sens. Spatial Inf. Sci.* ***2022***, 33–39.
11. Kumar, L.; Mutanga, O. Google Earth Engine Applications Since Inception: Usage, Trends, and Potential. *Remote Sens.* **2018**, *10*, 1–15, doi: 10.3390/rs10101509.
12. Azila, M.; Damai, A.A.; Asbi, A.M. Arahan Pemanfaatan Ruang Berbasis Mitigasi Bencana Banjir di Kecamatan Kelumbayan Kabupaten Tanggamus. *J. Planoearth* **2023**, *8*, 47–53, doi: 10.31764/jpe.v8i2.4765.
13. Paramita, B.; Matzarakis, A. Urban Biometeorology of Tropical Climate: Af, Am, Aw, a Propensity of 34 Provincial Cities in Indonesia. In *Climate Change and Cooling Cities*; Cheshmehzangi, A.; He, B.-J.; Sharifi, A.; Matzarakis, A., Eds.; Springer Nature Singapore: Singapore, 2023; pp. 283–296.
14. Badan Pusat Statistik Kota Pontianak. *Kota Pontianak dalam Angka 2024 (Pontianak Municipality in Figures 2024)*; Badan Pusat Statistik Kota Pontianak: Pontianak, ID, 2024.
15. Butar-Butar, R.B. *Bencana Banjir di Kota Pontianak Tahun 2004–2021*. Undergraduate Thesis, IKIP PGRI Pontianak, Pontianak, Indonesia, 2023.
16. Lillesand, T.M.; Kiefer, R.W.; Chipman, J.W. *Remote Sensing and Image Interpretation*, 7th ed.; John Wiley & Sons: Hoboken, NJ, USA, 2015.
17. Breiman, L. Random Forests. *Mach. Learn.* **2001**, *45*, 5–32, doi: 10.1023/A:1010933404324
18. Lolitasya, A.Y.; Hadi, M.Z.S.; Sa'adah, N. Development of a Real-Time Soil NPK Prediction System Using AS7265X Spectral Sensor and Random Forest Regression. In Proceedings of the 2025 International Electronics Symposium (IES), Surabaya, Indonesia, 5–7 August 2025; pp. 133–139.
19. Belgiu, M.; Drăguţ, L. Random Forest in Remote Sensing: A Review of Applications and Future Directions. *ISPRS J. Photogramm. Remote Sens.* **2016**, *114*, 24–31, doi: 10.1016/j.isprsjprs.2016.01.011.

20. Lange, T.M.; Gültas, M.; Schmitt, A.O.; Heinrich, F. optRF: Optimising Random Forest Stability by Determining the Optimal Number of Trees. *BMC Bioinformatics* **2025**, *26*, 1–21, doi: 10.1186/s12859-025-06097-1.

21. Ngurawan, M.G.R. *Analisis Sebaran Spasial Genangan Banjir Dengan Data Sentinel-1 Menggunakan Google Earth Engine (Studi Kasus: Kalimantan Selatan)*. Undergraduate Thesis, Institut Teknologi Sepuluh Nopember, Surabaya, Indonesia, 2021.

22. Lin, L.; Di, L.; Tang, J.; Yu, E.; Zhang, C.; Rahman, M.S.; Shrestha, R.; Kang, L. Improvement and Validation of NASA/MODIS NRT Global Flood Mapping. *Remote Sens.* **2019**, *11*, 205, doi: 10.3390/rs11020205.

23. Congalton, R.G. A Review of Assessing the Accuracy of Classifications of Remotely Sensed Data. *Remote Sens. Environ.* **1991**, *37*, 35–46, doi: 10.1016/0034-4257(91)90048-B

24. Natun, N.C.I.; Sumarlin. Analisis Perbandingan Klasifikasi Supervised dan Unsupervised Citra Satelit Landsat untuk Pemetaan Penutupan Lahan Di Kabupaten Kupang. *J. Manaj. Inform. Jayakarta* **2025**, *5*, 142–152, doi: 10.52362/jmijayakarta.v5i2.1812.

25. Olofsson, P.; Foodu, G.M.; Herold, M.; Steman, S.V; Woodcock, C.E.; Wulder, M.A. Good Practices for Estimating Area and Assessing Accuracy of Land Change. *Remote Sens. Environ.* **2014**, *148*, 42–57, doi: 10.1016/j.rse.2014.02.015.

26. Ahlqvist, O. Overlay (in GIS). In *International Encyclopedia of Human Geography*; Kitchin, R.; Thrift, N., Eds.; Elsevier: Oxford, UK, 2009; Volume 8, pp. 48–55.

27. Donchyts, G.; Schellekens, J.; Winsemius, H.; Eisemann, E.; van de Giesen, N. A 30 m Resolution Surface Water Mask Including Estimation of Positional and Thematic Differences Using Landsat 8, SRTM and OpenStreetMap: A Case Study in the Murray-Darling Basin, Australia. *Remote Sens.* **2016**, *8*, 103, doi: 10.3390/rs8050386

28. Mason, D.C.; Dance, S.L.; Cloke, H.L. Toward Improved Urban Flood Detection Using Sentinel-1: Dependence of the Ratio Of Post- to Pre-Flood Double Scattering Cross Sections on Building Orientation. *J. Appl. Remote Sens.* **2023**, *17*, doi: 10.1117/1.JRS.17.016507.

29. Abdo, R.; Ferro-Famil, L. PolSAR Analysis of Coherent and Diffuse Double-Bounce Scattering Occuring Within a Vegetated Medium. In Proceedings of the 2020 IEEE International Geoscience and Remote Sensing Symposium (IGARSS), Waikoloa, HI, USA, 26 September–2 October 2020; pp. 3865–3868.

30. Landis, J.R.; Koch, G.G. The Measurement of Observer Agreement for Categorical Data. *Biometrics* **1977**, *33*, 159–174, doi: 10.2307/2529310

31. Amin, R.; Rinanti, A.; Kurniyaningrum, E.; Anggraini, D.P.; Assidik, M.L. Implementation of Low Impact Development (Lid) for Urban Drainage Optimization and Flood Mitigation. *VOCATECH Vocat. Educ. Technol. J.* **2025**, *6*, 35–47, doi: 10.38038/vocatech.v6i2.204.

32. Palla, A.; Colli, M.; Candela, A.; Aronica, G.T.; Lanza, L.G. Pluvial Flooding in Urban Areas: The Role of Surface Drainage Efficiency. *J. Flood Risk Manag.* **2018**, *11*, S663–S676, doi: 10.1111/jfr3.12246.

33. Vozelj, U.; Šraj, M.; Bezak, N. Analysis of the Impact of Green Infrastructure on Surface Runoff From Urban Areas. *Acta hydrotechnica* **2023**, *36*, 111–121, doi: 10.15292/acta.hydro.2023.07.

34. Machado, F.; Vestena, L.R. Evolution of the Flood Mark and Built-up Areas in Flooded Lands in the City of Guarapuava, Paraná. *Rev. Geociências Do Nord.* **2024**, *10*, 537–550, doi: 10.21680/2447-3359.2024v10n1ID34910.

35. Malviya, A.; Dwivedi, A.; Manore, A.; Bamniya, A.; Sinha, A. A Conceptual Design Model to Groundwater Recharge in Dense Urban Area Roads. *Int. J. Innov. Technol. Explor. Eng.* **2020**, *9*, 751–755, doi: 10.35940/ijitee.G5480.059720.

36. Choi, J.; Harvey, J.W. Relative Significance of Microtopography and Vegetation as Controls on Surface Water Flow on a Low-Gradient Floodplain. *Wetlands* **2014**, *34*, 101–115, doi: 10.1007/s13157-013-0489-7.

37. Alves, R.M.C.; Lousada, S.A.N.; Cabezas, J.; Gómez, J.M.N. Urban Flooding Risk in Machico and Planning Its Territory as a Form of Prevention. *In Geoinformatics in Support of Urban Politics and the Development of Civil Engineering;* Neves Lousada, S.A., Ed.; IGI Global: Hershey, PA, USA, 2023; pp. 50–76.

38. Qin, X.; Shi, Q.; Member, S.; Wang, D.; Su, X. Inundation Impact on Croplands of 2020 Flood Event in Three Provinces of China. *IEEE J. Sel. Top. Appl. Earth Obs. Remote Sens.* **2022**, *15*, 3179–3189, doi: 10.1109/JSTARS.2022.3161320.
39. Monachese, A.P.; Gómez-Villarino, M.T.; López-Santiago, J.; Sanz, E.; Almeida-Ñauñay, A.F.; Zubelzu, S. Challenges and Innovations in Urban Drainage Systems: Sustainable Drainage Systems Focus. *Water* **2025**, *17*, 1–18, doi: 10.3390/w17010076.
40. Kartiwa, B.; Sutrisno, N.; Hamdani, A.; Nugroho, W.T.; Muhardiono, I.; Yani, I.; Roland, R.; Ismail, I. Polder system water management on non-tidal swamp area based on water balance analysis. *IOP Conf. Ser. Earth Environ. Sci.* **2021**, *648*, 012061.